tvst

DOI: 10.1167/tvst.5.4.11

Article

Optical Coherence Tomography Angiography in Mice: Comparison with Confocal Scanning Laser Microscopy and Fluorescein Angiography

Helena Giannakaki-Zimmermann*, Despina Kokona*, Sebastian Wolf, Andreas Ebneter, and Martin S. Zinkernagel

Department of Ophthalmology and Department of Clinical Research, Inselspital, Bern University Hospital, and University of Bern, Switzerland

Correspondence: Martin S. Zinkernagel, MD, PhD, Department of Ophthalmology, Inselspital, Bern University hospital, Universität Bern, CH-3010 Bern, Switzerland. email: martin.zinkernagel@insel.ch

Received: 21 March 2016
Accepted: 29 June 2016
Published: 18 August 2016

Keywords: optical coherence angiography; confocal microscopy; fluorescein angiography; confocal scanning microscopy; retinal vasculature

Citation: Giannakaki-Zimmermann H, Kokona D, Wolf S, Ebneter A, Zinkernagel MS. Optical coherence tomography angiography in mice: comparison with confocal scanning laser microscopy and fluorescein angiography. Trans Vis Sci Tech. 2016;5(4):11, doi:10.1167/tvst.5.4.11.

Purpose: Optical coherence tomography angiography (OCT-A) allows noninvasive visualization of retinal vessels in vivo. OCT-A was used to characterize the vascular network of the mouse retina and was compared with fluorescein angiography (FA) and histology.

Methods: In the present study, OCT-A based on a Heidelberg Engineering Spectralis system was used to investigate the vascular network in mice. Data was compared with FA and confocal microscopy of flat-mount histology stained with isolectin IB4. For quantitative analysis the National Cancer Institute's AngioTool software was used. Vessel density, the number of vessel junctions, and endpoints were measured and compared between the imaging modalities.

Results: The configuration of the superficial capillary network was comparable with OCT-A and flat-mount histology in BALBc mice. However, vessel density and the number of vessel junctions per region of interest ($P = 0.0161$ and $P = 0.0015$, respectively) in the deep vascular network of BALBc mice measured by OCT-A was significantly higher than with flat-mount histology. In C3A.Cg-*Pde6b*+*Prph2Rd2/J* mice, where the deep capillary plexus is absent, analysis of the superficial network provided similar results for all three imaging modalities.

Conclusion: OCT-A is a helpful imaging tool for noninvasive, in vivo imaging of the vascular plexus in mice. It may offer advantages over FA and confocal microscopy especially for imaging the deep vascular plexus.

Translational Relevance: The present study shows that OCT-A can be employed for small animal imaging to assess the vascular network and offers advantages over flat-mount histology and FA.

Introduction

The retina as part of the central nervous system offers the unique opportunity to directly image structural changes occurring in neurodegenerative and neurovascular diseases such as glaucoma or diabetic retinopathy.[1,2] Several animal models of retinal vascular diseases have provided information about the pathogenesis and potential therapeutic approaches such as retinal vein occlusion or oxygen-induced retinopathy.[3,4] A noninvasive imaging technique with the capability of detecting early vascular changes, such as capillary dropout, is paramount to develop treatment strategies for these potentially blinding diseases in small animal models.

Ex vivo techniques such as confocal scanning laser microscopy of retinal flat-mount specimens have been invaluable for studying the vascular network in the mouse but do not allow for sequential imaging. In the last years, several new imaging techniques such as scanning laser ophthalmoscopy have been adapted from clinical use to study the rodent retinal vasculature and to perform longitudinal studies of the retinal vasculature in rodents.[5] However, conventional imaging methods such as fluorescein angiography (FA) provide only incomplete morphologic information

about the deep vascular plexus (DVP).[6,7] This shortcoming can be overcome by spectral-domain optical coherence tomography angiography (OCT-A) as it combines cross-sectional intensity based structural information of the retina using high-resolution spectral-domain OCT (SD-OCT) with information on blood flow. High-resolution SD-OCT is able to acquire three-dimensional (3D) images resolving the microstructures of the rodent retina, similar to histology. OCT-A is increasingly used in clinics to study microvascular pathology in various retinal diseases and more recently it has been used for the evaluation on choroidal neovascularization in mice.[8–10] Using OCT-A, individual retinal layers can be segmented and therefore information on the location of microvascular changes can be obtained.

In this study, we aimed to determine if the various layers of the mouse retinal vasculature can be visualized spectral-domain–based OCT-A and how these images compare with FA (Heidelberg Spectralis Retinal Angiography, HRA) and confocal laser scanning microscopy of IB4 stained flat-mount sections.

Methods

Animals

Thirteen BALB/c (wild-type inbred strain, nonpigmented, 4- to 6-weeks old) and two mice with an *rd2* mutation (C3A.Cg-*Pde6b+Prph2Rd2/J*, 6-months old) were used in this study. Mice homozygous for the *rd2,* or retinal degeneration slow *(rds)* mutation display a degeneration of the outer nuclear layer of the retina beginning at 5 weeks and loss of all visual cell structures by 12 months of age.[11] Animals were kept at the breeding facility of the Department of Clinical Research, University Hospital of Bern, under pathogen-free conditions in individually ventilated cages with a standard 12-hour:12-hour light–dark cycle with food and water available ad libitum. All animals were treated according to the ARVO Statement for the Use of Animals in Ophthalmic and Vision Research and after governmental approval according to the Federal Swiss Regulations on Animal Welfare.

Anaesthesia was performed subcutaneously by injecting 45 mg/kg ketamine (Ketalar 50 mg/ml; Orion Pharma AG, Zug, Zurich, Switzerland) and 0.75 mg/kg medetomidine hydrochloride (Dormitor, 1 mg/ml; Orion Pharma AG). After image acquisition, 0.75 mg/kg atipamezole (Antisedan 5 mg/ml; Orion Pharma AG) was given to reverse anaesthesia. The use of medetomidine hydrochloride instead of xylazine enabled us to perform the imaging, and thus no additional anaesthetics were considered necessary. Pupils were dilated using tropicamide 0.5% and phenylephrine HCl 2.5% (ISPI, Bern, Switzerland). To prevent drying or damage to the cornea due to the lack of blinking once the mice are asleep, hydroxypropylmethylcellulose (Methocel 2%; OmniVision, Neuhausen, Switzerland) was applied to each eye during imaging.

Imaging

In order to obtain a good view of the fundus of the eye, mice were placed on a custom-made platform. To prevent hypothermia, a warming patch of approximately 32°C was placed between the mouse and the platform. All images were taken and measurements done by a SD- OCT device Heidelberg Engineering (HRA Spectralis system; Heidelberg Engineering, Heidelberg, Germany) using a 55° lens (Fig. 1A). A contact lens was not used during image acquisition.

Fluorescein Angiography

As contrast agent, 0.5 mg of fluorescein (5 μL of undiluted Fluorescein 10% Faure; Novartis, Switzerland; + 45 μL water for injection) was administered intraperitoneally 3 to 5 seconds before image acquisition. Images were performed using the high-definition mode of the HRA system and a 55° lens. The large vessels were brought into focus in the infrared mode and a further adjustment was made after switching to FA mode to compensate for chromatic aberration to bring the vessels into better focus.

OCT Angiography

A Spectralis OCT-A prototype operating at 70 kHz was used. Image size of 3.8 × 1.9 mm (scaled for humans and not for mice) with 13 images averaged per scan was selected. The number of total B-scans then calculated by the software was approximately 391 images – the distance between the B-scans was 5 to 6 μm.

Immunohistochemical Studies

After imaging, the mice were euthanized with CO_2 inhalation and their eyes were removed and fixed in 4% parafolmaldehyde solution (PFA, pH 7.4) for 10 minutes. The anterior segments (cornea and lens) were removed and the whole retina was dissected from the eyecup and incubated for 50 more minutes in

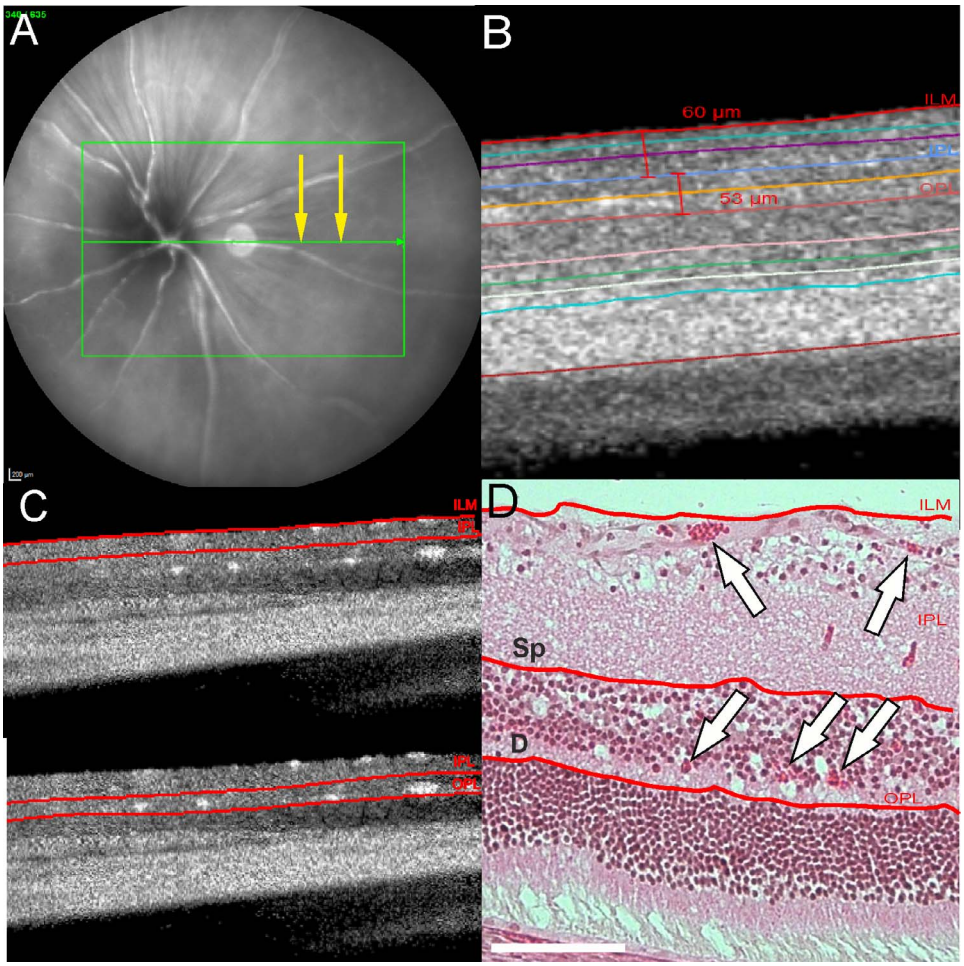

Figure 1. Location of the superficial and deep plexus in the mouse retina. (A) Infrared fundus picture of the posterior pole of the mouse eye imaged with the OCT-A device. *Yellow arrows* indicate the selected area of the B-scan presented in (B). (B) Automatic segmentation of retinal layers using the Heidelberg Eye Explorer Software. The distance between the ILM and the IPL and between the IPL and the OPL was manually measured. (C) Based on the thickness measurements in (B) manual retinal layer segmentation was possible for the identification of the SVP (*upper panel*) and DVP (*lower panel*) located between the ILM and the outer boundary of the IPL and between the IPL and the outer boundary of the OPL, respectively. (D) Superficial (*Sp*) and deep (*D*) vessels are also visible in histology in the same retinal layers as described above. *Arrows* indicate vertical cuts of vessels in each layer. *Scale bar*, 100 µm.

4% PFA. Fixed retinas were extensively washed in 0.1% Triton in phosphate buffer solution (PBS) and incubated in blocking buffer (5% normal goat serum [NGS] in 0.1% Triton in PBS) for 2 hours at room temperature. Retinas were incubated in Isolectin GS-IB4 antibody from *Griffonia simplicifolia*, Alexa Fluor 647 conjugate (1:100 in blocking buffer; Thermo Fisher Scientific, Waltham, MA) at 4°C for 48 hours on a shaker, for the labelling of blood vessels. The retinas were rinsed four more times with PBS-0.1% Triton, four radial cuts were made and the tissues were flat-mounted on a slide with the ganglion cell layer facing up. Flat-mounts were cover-slipped and observed in an inverted Zeiss LSM 710 fluorescence confocal microscope (Carl Zeiss, Oberkochen, Germany). Z-stacks of 83.2 ± 36.4 µm of tissue (mean ± standard error of the mean [SEM]) with 1 µm interval, containing both the superficial and DVP, were obtained and analyzed with the ZEN system 2011 software (Carl Zeiss).

Retinal Layer Segmentation to Identify Vascular Planes

The OCT-A prototype applied the same 11-layer segmentation algorithm as it is available for regular OCT imaging which is able to identify reference planes in OCT scans of healthy eyes.[12] The Spectralis OCT-A device automatically localizes the superficial vascular plexus (SVP) between the inner limiting

membrane (ILM) and the outer boundary of the inner plexiform layer (IPL), whereas the deep retinal plexus is localized between the outer boundary of the IPL and the outer boundary of the outer plexiform layer (OPL).[12] Because of different dimensions in the mouse retina some adjustments to the above mentioned thickness profiles were necessary and the segmentation lines for the SVP were manually set from the ILM to the outer boundary of the IPL, which corresponds to approximately 60 μm (Fig. 1B).[13] The DVP was defined between the IPL and the outer boundary of the OPL (Figs. 1A–C).

In keeping with previous reports mice with a *rd2* mutation had a much thinner retina (mean thickness we measured: 72.9 μm ± 1.1 SD), and the segmentation lines for the DVP were set in the area below the IPL.[11]

Analysis of Vessel Density

In order to calculate vessel density we used AngioTool software (National Institute of Health National Cancer Institute, Gaithersburg, MD).[14] To avoid bias, the main vessels were excluded from analysis. To assess the performance of OCT-A to image the vascular network in the SVP and DVP we compared OCT-A with confocal scanning laser microscopy of flat-mount specimens stained for IB4. With confocal microscopy, both, the superficial and the deep plexus of the mouse retina can be differentiated by scrolling through the z-stack axis providing some 3D information of the vascular network. For quantitative comparison of the three imaging modalities we chose vessel density (%), number of endpoints per section, and number of junctions per region of interest. These features were analyzed separately for both the SVP and the DVP in OCT-A and confocal microscopy, whereas in FA we did not differentiate individual plexi. The same area within the retina was chosen for comparison of the imaging modalities and a total area of 1.3 ± 0.15 mm^2 was measured per image calculated from the flat-mounts.

Despite the confocality of the microscope, there was still considerable overlay of the superficial vasculature in the DVP. Therefore, we subtracted the superficial vessel density from the total vessel density obtained from confocal scanning laser microscopy.

Statistical Analysis

Data was collected in tables and statistical analysis was then performed using Prism Graph Pad commercial software (Prism 6; GraphPad Software Inc., La Jolla, CA). Data was analyzed using unpaired *t*-tests. For all analyses *P* less than 0.05 was considered statistically significant. All results are presented as mean ± SEM.

Results

Imaging of the Retinal Vasculature Using OCT-A in BALB/c Mice

Because of breathing movements of the anesthetized mouse and the small size of the eye image acquisition took approximately 15 minutes to perform imaging procedures. The mean retinal thickness in BALBc mice was 208.16 μm ± 9.31 SD.

In BALB/c mice two distinct vascular networks were identifiable within the retina. Decorrelation of OCT scans (Fig. 1C) revealed vessels between the ILM and the outer boundary of the IPL corresponding to the SVP, whereas the DVP was found between the IPL and the outer boundary of the OPL, which is in keeping with hematoxylin and eosin histology where vessel lumens of these two plexus can be distinguished in between these layers (Fig. 1D). When computing the decorrelation OCT scan as en face images, based on concatenation of images taken in the vertical level, the presence of these two main layers of retinal vasculature (Figs. 2A, 2B, SVP and DVP, respectively) was visible. Whereas the SVP and the DVP were clearly visible in retinal flat-mounts (Fig. 2D), FA did not allow differentiating morphologic information on individual plexi (Fig. 2C).

Quantification of Vessel Density

There was no significant difference in vessel density, number of junctions, and endpoints (number of open-ended segments) when analyzing the superficial plexus in the OCT-A and confocal scanning laser microscopy. However, analysis of the DVP showed significant differences in all three features, with all of them being significantly lower in confocal scanning laser microscopy compared to OCT-A (Fig. 3). Because individual layers could not be differentiate in FA and because FA only provides incomplete morphological information on the DVP we analyzed FA data as SVP. FA data showed a larger vessel area than the SVP data of OCT-A or confocal scanning microscopy (Fig. 3C). This is probably due to some influence from the DVP.

In C3A.Cg-*Pde6b*+ *Prph2Rd2*/*J* mice the SVP had

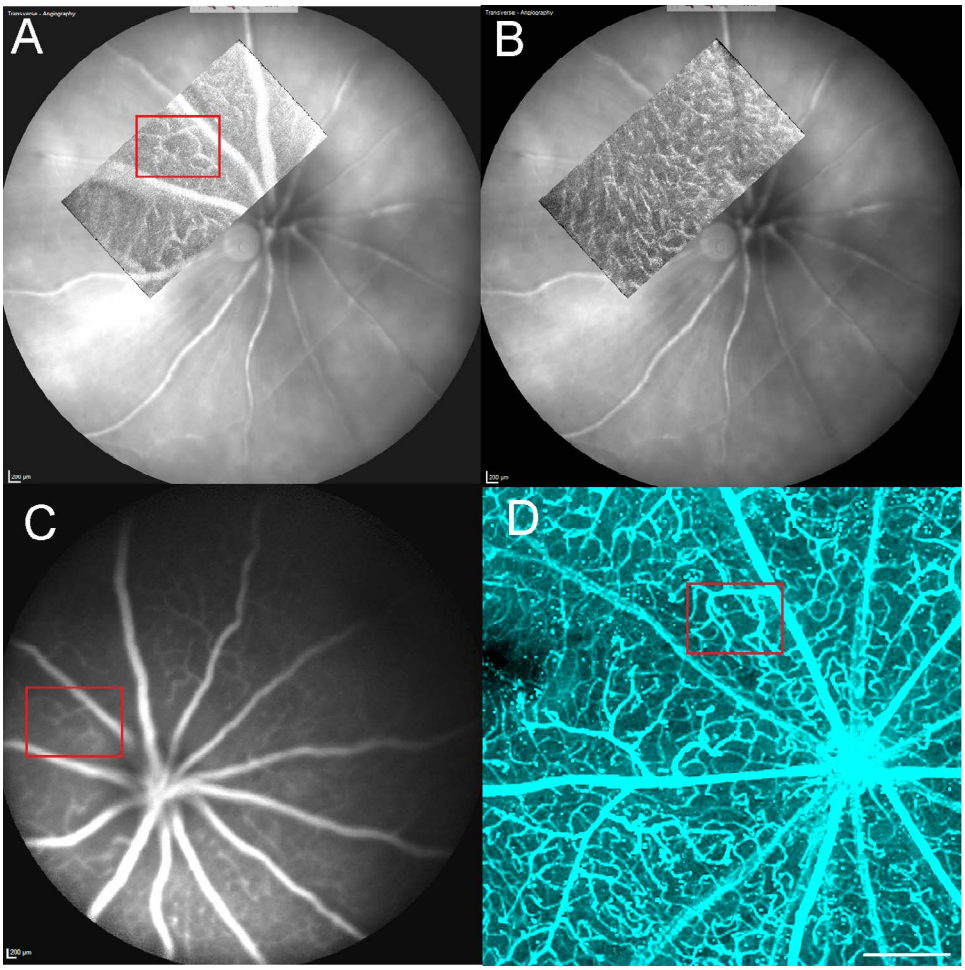

Figure 2. Comparison of the retinal vasculature using different imaging modalities. SVP (A) and DVP (B) of the mouse retina obtained with OCT-A (A, B) FA (C), or confocal microscopy ([D] *Scale bar*, 100 μm). *Red square* delineates the corresponding areas of the superficial plexus that could be visualized in all three imaging modalities ($n = 13$).

similar features as in wild-type mice in OCT-A (Figs. 4A, 4B, *rd2* and wild-type mouse, respectively). However, the DVP was absent in all of the image acquisition modalities, which is in keeping with published data using histology.[15] Quantification of vessel density, number of junctions, and endpoints showed similar values in OCT-A, histology, and FA (Fig. 4C).

Discussion

In mice and humans, the entire retina is vascularized, with blood flow directed from the optic disc radially to the periphery of the retina.[16] The central retinal artery, being supplied from the internal carotid artery, branches in four to eight retinal arterioles, depending on the mouse strain.[17,18] The retinal microvasculature consists of two distinct vascular layers: a superficial capillary layer in the nerve fiber/ganglion cell layer, and the deeper capillary layer extending into the inner nuclear and outer plexiform layers.[19] In the mouse, it has been shown that the superficial plexus consists mostly of arterioles, which branch into three to four precapillary arterioles.[20] In contrast, the DVP is predominantly venous and consists of mostly capillaries.[12] Recent studies have differentiated three different vascular planes within the mouse retina, the intermediate layer (within the IPL) being the connection between the superficial and the DVP with mostly perpendicular divisions of the vessels, and thus being the less distinct one.[20,21] In order to clearly differentiate vessel structures of the deep and superficial plexus we avoided placing the slabs for the different planes too closely, and therefore did not

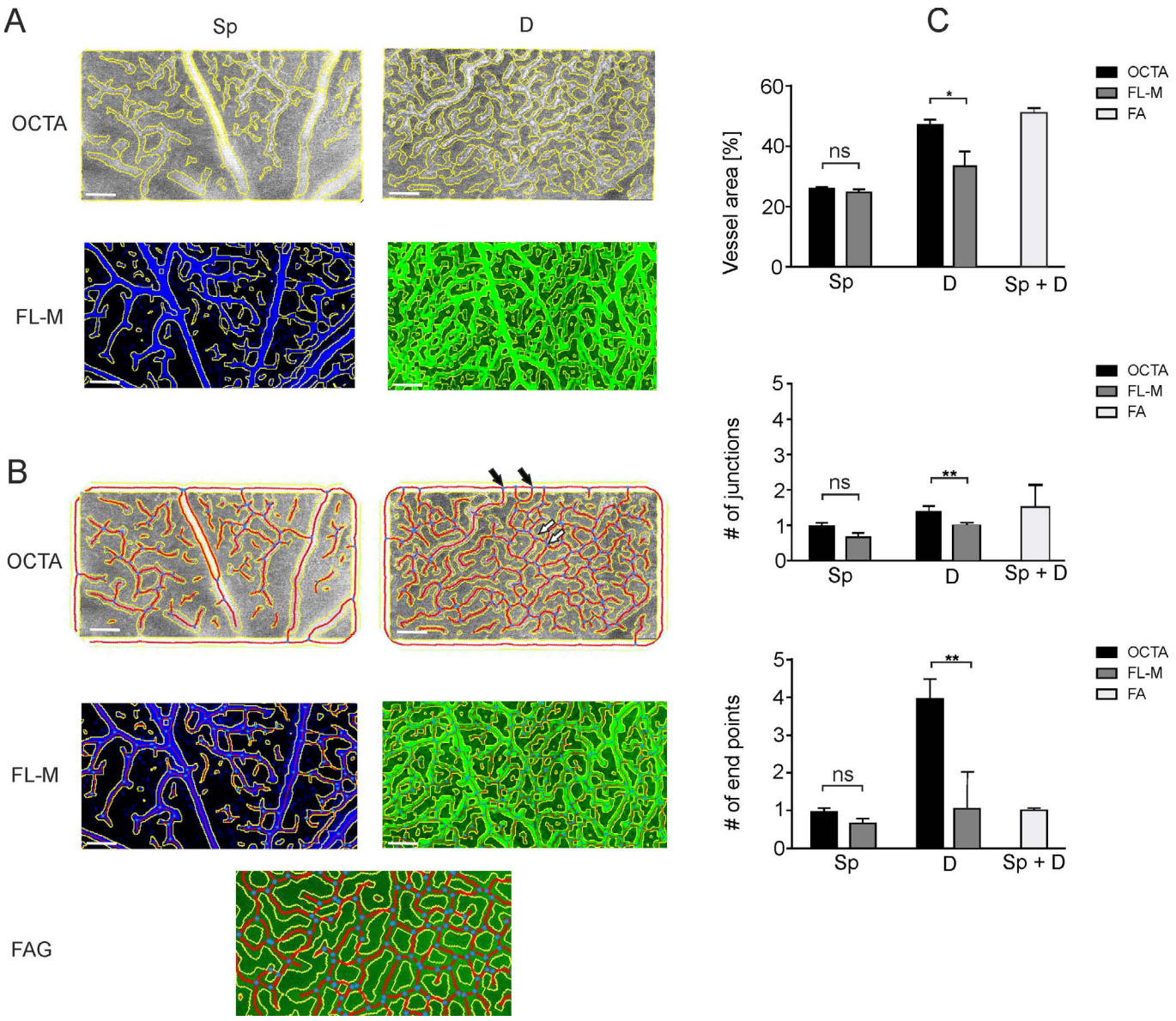

Figure 3. Analysis of different features of the retinal vasculature using the AngioTool software. (A) Vessels of the superficial (Sp, *left panel*) and the deep (D, *right panel*) vasculature were automatically outlined using the AngioTool software, indicated by the *yellow lines* surrounding the vessels. Both OCT-A (*upper panel*) and flat-mount (*bottom panel*) pictures were included. In FA images (FAG) both the SVP and DVP were included in the quantification. (B) After the delineation of retinal vessels, the AngioTool software automatically calculated vessel density (*red lines*), number of end points (*blue dots* indicated with *dark arrows*) and number of junctions (*blue dots* indicated with *white arrows*). *Scale bar*, 100 μm. (C) Bar graphs were generated with GraphPad Prism and analyzed using unpaired *t*-tests. No statistically significant difference was observed comparing the superficial plexus calculated from OCT-A or flat-mounts, concerning vessels density, end points, and number of junctions. However, comparing the same values in the deep plexus we observed significant differences between OCT-A and flat-mounts (number of junctions: $P = 0.0015$; number of endpoints: $P = 0.0071$), although the vessel density showed less discrepancy ($P = 0.0166$). FA was not included in the quantification: the bar graph shows the absolute values of both the Sp and D plexus as the layers were not separately analyzed.

include the intermediate vascular plexus in our analysis.

Visualizing the vasculature of the retina is paramount in order to dissect the pathomechanisms of vascular eye diseases such as retinal vein occlusion, retinal artery occlusion, or diabetic retinopathy. Histology has long been considered the gold standard for assessing and quantifying

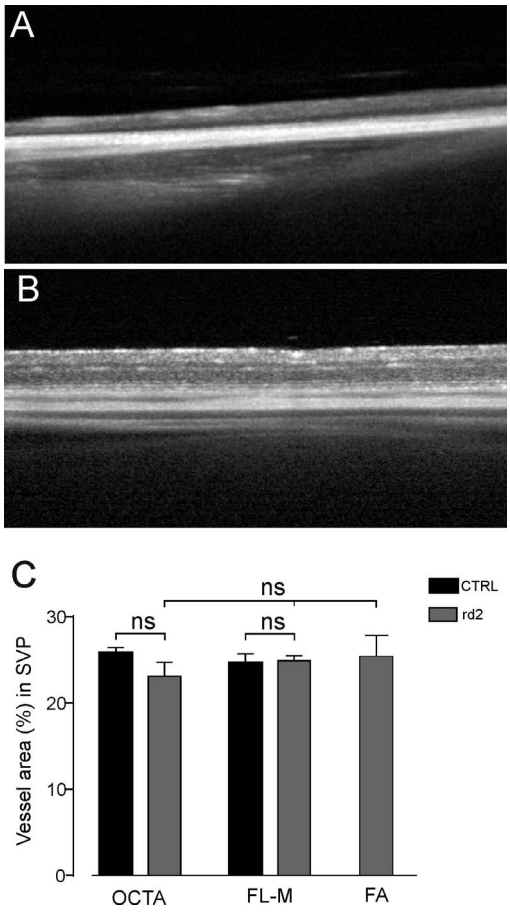

Figure 4. OCT-A imaging of C3A.Cg-*Pde6b*+*Prph2Rd2/J* mice. (A, B) Representative images illustrate retinal thickness in C3A.Cg-*Pde6b*+*Prph2Rd2/J* (A) mice and wild-type mice (B), respectively. (C) Vessel area (%) in SVP of wild-type mice and C3A.Cg-*Pde6b*+*Prph2Rd2/J* mice. No statistically significant difference in vessel density was observed comparing FA with OCT-A or flat-mount histology (unpaired *t*-test, ns, not significant).

vascular changes in animal models, as well as for judging the efficacy of potential treatments.[22] Immunostaining of vascular endothelium with fluorophore-labeled isolectin B4 in retinal flat-mounts can highlight the overall architecture of the retinal vessels.

However, there are many disadvantages associated with histologic processing. Because of the inherent need to sacrifice animals to obtain histologic data, a large number of animals are needed to analyze sequential time points in a long-term study. Quantitative assessment of the vascular network ex vivo can be problematic due to the nonlinear artifacts induced by fixation, postmortem ischemia, or tissue processing. Despite excellent resolution of confocal microscopy to image retinal vessels, the deeper vascular networks are often difficult to differentiate from the superficial layers. Additionally, because of the interindividual variability of many animal models of vascular diseases, it would be desirable to test therapeutic approaches in the same animal.[23,24] In this direction, the normal vasculature in C57BL/6J mice was recently evaluated with OCT-A using an RTVue XR Avanti system (Optovue, Inc., Fremont, California).[10] Furthermore, this study showed that OCT-A was useful to visualize laser-induced choroidal neovascularization in mice. However, so far, a comparison of OCT-A findings and histology of the retinal vasculature has not been performed.

The principle of OCT-A is based on image decorrelation, where particles in motion are subtracted from static ones by taking a series of high speed pictures. The inter B-scan time, which is the time that passes between two consecutive B-scan acquisitions, is crucial for the detection of blood flow. OCT using split-spectrum amplitude-decorrelation angiography (SSADA) is able to detect normal capillary flow speeds, which have been estimated at between 0.4 and 3 mm/s and which is in the range of 1.26 ± 0.34 mm/s that has been reported in retinal vessels in mice.[25–28] If blood flow is slower than the B-scan time between consecutive B scans, no signal can be detected at all. In order to compare morphological features between the three imaging modalities, we analyzed the vascular density in the superficial and DVP using AngioTool software.[14,20] Because lateral measurements using OCT have been shown to be inaccurate in mice we were not able to use the scale bars provided in the infrared images corresponding to the OCT scans.[29] Instead, we identified matching areas in histology to FA and OCTA. There are no available reports about vascular degeneration in *rd2* mice. However, similar to mice with *rd1* mutations the outer nuclear layer degenerates, albeit slower than in *rd1* mice.[11] In *rd1* mice the DVP degenerates by the end of the second postnatal week coinciding with the degeneration of the outer retinal layers.[29] Here, we found that the DVP is absent in 6-month-old C3A.Cg-*Pde6b*+ *Prph2Rd2*/*J* mice. This allowed comparing morphological features of the SVP without potential interference from the DVP.[15,30] Here, we found that all three imaging modalities provided similar information on morphological features of the SVP.

There are several limitations when applying OCT devices designed for clinical use in small animal models. Image acquisition was protracted because of

decreased performance of the tracking feature due breathing artefacts. Furthermore, there are some limitations due to the short axial length of the mouse eye, which is only approximately 3 mm, and therefore considerably smaller than the human eye.[31] This leads to image disparity toward the periphery due to the higher convexity of the mouse eye and therefore OCT-A measurements can only be performed of the posterior pole of the mouse eye. Another limitation inherent to OCT-A technology is projection artifacts, where artifactual images may be projected into deeper retinal layers than they actually are. This may lead to a higher vessel density in the DVP.

Lastly, because lateral measurements are inaccurate in the mouse eye in OCT and infrared images, we had to approximate regions of interests for quantification in the three imaging modalities.

Our report combined with the recent application of OCT-A for the evaluation of experimental choroidal neovascularization in mice serves as a proof of concept that OCT-A may be used to obtain in vivo information on animal models to study retinal vascular abnormalities following photoreceptor loss and may provide new information on disease models for retinal dystrophies.[10]

Conclusion

Our report confirms the feasibility of OCT-A imaging in the mouse. Our results suggest that especially for the deeper vascular network OCT-A imaging may provide more details than confocal microscopy, and therefore may be especially suited to obtain new insights of vascular changes in mouse models of retinal dystrophies, such as retinitis pigmentosa, where the outer retinal layers are affected.

Acknowledgments

Supported by a grant of the Swiss National Science Foundation (SNSF; #320030_156019). The authors received nonfinancial support from Heidelberg Engineering GmbH, Germany

*Helena Giannakaki-Zimmermann and Despina Kokona contributed equally to this work.

Disclosure: **H. Giannakaki-Zimmermann,** None; **D. Kokona,** None; **S. Wolf,** Heidelberg Engineering (Consultant, nonfinancial support); **A. Ebneter,** None; **M.S. Zinkernagel,** Heidelberg Engineering (nonfinancial support)

References

1. Zhang X, Francis BA, Dastiridou A, et al. Longitudinal and cross-sectional analyses of age effects on retinal nerve fiber layer and ganglion cell complex thickness by Fourier-domain OCT. *Transl Vis Sci Technol*. 2016;5:1.
2. Ebneter A, Wolf S, Abhishek J, Zinkernagel MS. Retinal layer response to ranibizumab during treatment of diabetic macular edema: thinner is not always better. *Retina*. 2016;36:1314–1323.
3. Ebneter A, Agca C, Dysli C, Zinkernagel MS. Investigation of retinal morphology alterations using spectral domain optical coherence tomography in a mouse model of retinal branch and central retinal vein occlusion. *PloS One*. 2015;10: e0119046.
4. Smith LE, Wesolowski E, McLellan A, et al. Oxygen-induced retinopathy in the mouse. *Invest Ophthalmol Vis Sci*. 1994;35:101–111.
5. Kim KH, Puoris'haag M, Maguluri GN, et al. Monitoring mouse retinal degeneration with high-resolution spectral-domain optical coherence tomography. *J Vis*. 2008;8:17.1–11.
6. Weinhaus RS, Burke JM, Delori FC, Snodderly DM. Comparison of fluorescein angiography with microvascular anatomy of macaque retinas. *Exp Eye Res*. 1995;61:1–16.
7. Mendis KR, Balaratnasingam C, Yu P, et al. Correlation of histologic and clinical images to determine the diagnostic value of fluorescein angiography for studying retinal capillary detail. *Invest Ophthalmol Vis Sci*. 2010;51:5864–5869.
8. Spaide RF. Volume-rendered optical coherence tomography of diabetic retinopathy pilot study. *Am J Ophthalmol*. 2015;160:1200–1210.
9. Spaide RF, Klancnik JM Jr, Cooney MJ. Retinal vascular layers imaged by fluorescein angiography and optical coherence tomography angiography. *JAMA Ophthalmol*. 2015;133:45–50.
10. Alnawaiseh M, Rosentreter A, Hillmann A, et al. OCT angiography in the mouse: a novel evaluation method for vascular pathologies of the mouse retina. *Exp Eye Res*. 2016;145:417–423.
11. Chang B, Hawes NL, Hurd RE, Davisson MT, Nusinowitz S, Heckenlively JR. Retinal degeneration mutants in the mouse. *Vision Res*. 2002;42: 517–525.

12. Harris A, Jonescu-Cuypers CP, Kagemann L, Ciulla TA, Krieglstein K. *Atlas of ocular blood flow: vascular anatomy, pathophysiology, and metabolism*. Phildelphia: Butterworth-Heinemann; 2003:128 pp.
13. Dysli C, Enzmann V, Sznitman R, Zinkernagel MS. Quantitative analysis of mouse retinal layers using automated segmentation of spectral domain optical coherence tomography images. *Transl Vis Sci Technol*. 2015;4:9.
14. Zudaire E, Gambardella L, Kurcz C, Vermeren S. A computational tool for quantitative analysis of vascular networks. *PloS One*. 2011;6:e27385.
15. Pennesi ME, Nishikawa S, Matthes MT, Yasumura D, LaVail MM. The relationship of photoreceptor degeneration to retinal vascular development and loss in mutant rhodopsin transgenic and RCS rats. *Exp Eye Res*. 2008;87:561–570.
16. Germer A, Biedermann B, Wolburg H, et al. Distribution of mitochondria within Müller cells–I. Correlation with retinal vascularization in different mammalian species. *J Neurocytol*. 1998;27:329–345.
17. Saint-Geniez M, D'Amore PA. Development and pathology of the hyaloid, choroidal and retinal vasculature. *Int J Dev Biol*. 2004;48:1045–1058.
18. Smith RS, John SWM, Nishina PM, Sundberg JP. *Systematic evaluation of the mouse eye: anatomy, pathology, and biomethods*. Boca Raton, FL: CRC Press, Inc.; 2002:384 pp.
19. Toussaint D, Kuwabara T, Cogan DG. Retinal vascular patterns. II. Human retinal vessels studied in three dimensions. *Arch Ophthalmol*. 1961;65:575–581.
20. McLenachan S, Magno AL, Ramos D, et al. Angiography reveals novel features of the retinal vasculature in healthy and diabetic mice. *Exp Eye Res*. 2015;138:6–21.
21. Kornfield TE, Newman EA. Regulation of blood flow in the retinal trilaminar vascular network. *J Neurosci*. 2014;34:11504–11513.
22. Silberstein EB. Cancer diagnosis. The role of tumor-imaging radiopharmaceuticals. *Am J Med*. 1976;60:226–237.
23. Crespo-Garcia S, Reichhart N, Hernandez-Matas C, et al. In vivo analysis of the time and spatial activation pattern of microglia in the retina following laser-induced choroidal neovascularization. *Exp Eye Res*. 2015;139:13–21.
24. Van Bergen T, Spangler R, Marshall D, et al. The role of LOX and LOXL2 in the pathogenesis of an experimental model of choroidal neovascularization. *Invest Ophthalmol Vis Sci*. 2015;56:5280–5289.
25. Riva CE, Petrig B. Blue field entoptic phenomenon and blood velocity in the retinal capillaries. *J Opt Soc Am*. 1980;70:1234–1238.
26. Tam J, Tiruveedhula P, Roorda A. Characterization of single-file flow through human retinal parafoveal capillaries using an adaptive optics scanning laser ophthalmoscope. *Biomed Opt Express*. 2011;2:781–793.
27. Jia Y, Bailey ST, Hwang TS, et al. Quantitative optical coherence tomography angiography of vascular abnormalities in the living human eye. *Proc Natl Acad Sci U S A*. 2015;112:E2395–E2402.
28. Paques M, Tadayoni R, Sercombe R, et al. Structural and hemodynamic analysis of the mouse retinal microcirculation. *Invest Ophthalmol Vis Sci*. 2003;44:4960–4967.
29. Lozano DC, Twa MD. Development of a rat schematic eye from in vivo biometry and the correction of lateral magnification in SD-OCT imaging. *Invest Ophthalmol Vis Sci*. 2013;54:6446–6455.
30. Blanks JC, Johnson LV. Vascular atrophy in the retinal degenerative rd mouse. *J Comp Neurol*. 1986;254:543–553.
31. Park H, Qazi Y, Tan C, et al. Assessment of axial length measurements in mouse eyes. *Optom Vis Sci*. 2012;89:296–303.